Clinics in Surgery

Research Article
Published: 22 Jun, 2021

Properties Extracellular Action Potentials from Posteromedial Hypothalamus

Jesús Pastor[1,2,], Lorena Vega-Zelaya[1,2] and Elena Martín Abad[1,2]*

[1]Clinical Neurophysiology, Hospital Universitario La Princesa, Diego de León, Spain

[2]Foundation for Biomedical Research, Diego de León, Spain

Abstract

We have described the electrophysiological properties of the Extracellular Action Potential (EAP) picked up through Microelectrode-Recordings (MERs) from four patients operated under general anaesthesia at Postero-Medial Hypothalamus (PMH) by Deep Brain Stimulation (DBS) for erethism. EAPs from the same cell were pooled to obtain a mean EAP (mAP). The amplitudes and durations for all 2/3 phases were computed from the mAP, together with the maximum (dV_{max}) and minimum (dV_{min}) values of the first derivative. mAPs are denominated according to the phase polarity (P/N for positive/negative). We obtained a total 159 mAPs, all of them positive and a clear majority triphasic (89.9%) with a small P/N deflection (V1) before depolarization. The percentage of the different types of mAPs was surprisingly similar to that described recently at thalamus and although were some properties as peak-to-peak amplitude or overall duration. We observed a high correlation between absolute amplitude of the first phase (V1) and the amplitudes of either depolarization (V2) or repolarization (V3) phases, meaning that a causal relationship between them probably exists. We postulate capacitive current as responsible for V1, although it's difficult to explain the appearing of the same polarity for the capacitive voltage and for the voltage induced by transmembrane ionic current.

Keywords: Agglomerative method; Aggressiveness; Capacitive current; Deep brain stimulation; erethism; Microelectrode recordings; Sorting spikes

Introduction

Erethism describes severe cases of unprovoked aggressive behaviour, usually associated with some degree of mental impairment and gross brain damage [1]. The etiology can be due to perinatal insults, brain malformation, postencephalitic, posttraumatic or epileptic and usually is accompanied by hyperkinesia, self-aggressiveness and destructiveness of objects. Patients usually need to be institutionalized and managed with major restraining measures. A successful surgical treatment initially was the posteromedial hypothalamus [1,2]. Deep Brain Stimulation (DBS) at Posteromedial Hypothalamus (PMH) has widely replaced the ablative procedures because the clinical benefits appear to be similar, but the treatment can be titrated and is also reversible, with a low risk of complications [3-6].

The human hypothalamus is a complex structure composed of different nuclear groups [7]. However, in general, there are no anatomical landmarks to identify a nucleus at the millimetric range. Nevertheless, the identification of hypothalamic nuclei is particularly important to obtain a good functional outcome in Deep Brain Stimulation (DBS) to optimize battery life and decrease secondary effects, especially considering that very sensible nuclei related to arousal, circadian rhythm or hormones-release are very close. So little is known about the electrophysiological properties of hypothalamus [5,8] and nothing about the features of Extracellular Action Potentials (EAP) obtained from this structure.

Microelectrode Recording (MER) is a useful tool used during DBS surgery to identify deep brain nuclei [9-11]. When surgery is performed in thalamic, subthalamic or globus pallidus, in addition to MER, other physiological tests can be performed to identify nuclei, such as cellular responses to voluntary or passive movements, tactile stimulus or paraesthesia induced by electrical stimulation [12-14]. However, in hypothalamus these stimuli are not useful, and the only electrophysiological help is the electrical stimulation [3,5].

Nonetheless, most of the information obtained during MER in clinical practice is restricted

OPEN ACCESS

Correspondence:
Jesús Pastor, Clinical Neurophysiology, Hospital Universitario La Princesa, Diego de León, 62, Madrid, Spain, E-mail: jesus.pastor@salud.madrid.org

Received Date: *29 May 2021*
Accepted Date: *15 Jun 2021*
Published Date: *22 Jun 2021*

Citation:
Pastor J, Vega-Zelaya L, Martín Abad E. Properties Extracellular Action Potentials from Posteromedial Hypothalamus. Clin Surg. 2021; 6: 3224.

Copyright *© 2021 Jesús Pastor. This is an open access article distributed under the Creative Commons Attribution License, which permits unrestricted use, distribution, and reproduction in any medium, provided the original work is properly cited.*

to the mean frequency of discharge and firing pattern (e.g., tonic, phasic, or more or less paused) [8,11,15-17], considering the EAP as a bimodal variable (present or absent) that is represented as a vertical line without an inner structure in binary plots, under the assumption that the morphology of an AP does not carry any information [18]. However, we have recently demonstrated that different types of EAP can be obtained from thalamus and the differential distribution could be helpful to identify specifically every structure, although this possibility has not been demonstrated [10].

The aim of our study was applying the same EAP analysis to hypothalamic MER performed in four patients treated by pathological aggressiveness to characterize the properties of EAP from PMH. We are not interested in analysis of pattern discharge.

Materials and Methods

Patients

We studied 4 patients undergoing DBS treatment at PMH for intractable aggressivity (Table 1 for clinical information). The experimental procedure was approved by the medical ethics review board of the Hospital Universitario de La Princesa and was deemed "care as usual". Under these circumstances, written informed consent was not required because all procedures were done by clinical necessity and analysis was off-line.

Surgical procedures

All the patients were operated on while under general anaesthesia using propofol (5.48 ± 0.28 mg/kg/h, (4.5, 6.2)) and remifentanil (0.12 ± 0.02 μg/kg/min, (0.1, 0.2)), maintaining a bi-spectral index between 40 and 45. Neuromuscular blockade during intubation was accomplished with cisatracurium (0.5 mg/kg).

The hypothalamus was identified using a 1.5 T magnetic resonance imaging (MRI, General Electric®, Fairfield, CT, USA), and the coordinates were located stereotactically with a neuronavigator (BrainLab®, Feldkirchen, Germany). The coordinates were calculated by fusing the MRI image and computed tomography scan according to the Schaltenbrand-Wahren map (SW [19]). For thalamic DBS electrode placement, a tentative initial target was selected in the posterolateral hypothalamus according to the Sano's triangle (x=2, y=0, z= -2). All the coordinates (in mm) refer to the mid-intercommissural AC-PC line (Anterior Commissure-Posterior Commissure). Neuronal recordings (Leadpoint®, Minneapolis, MN, USA) were obtained beginning 10 mm above the target and progressing in steps of 0.5 mm. MERs (FHC®, Maine, USA) were obtained until 2 mm below the theoretical target. Impedance was always above 900 kΩ (1696 kΩ ± 80 kΩ, (900, 2900)).

MERs were obtained through 3 to 4 microelectrodes separated by 2 mm. A microdrive was fixed to a stereotactic Leksell Coordinate Frame (Elekta®, Stockholm, Sweden). The bandwidth for spontaneous activity was 200 Hz to 5 kHz, with a sample rate of 24 kHz. The notch filter was off. PMH region was identified by MER and response to electrical stimulation [3,5]. After the PMH was identified, a quadripolar DBS electrode was implanted (Figure 1A), with a programmable stimulator placed in a pectoral or abdominal location.

The reconstruction of the trajectory was described in detail elsewhere [14]. Anteroposterior and lateral coordinates were obtained from the post-op MRI performed one month after surgery. Using these points and the stereo-tactic angles, we reconstructed the real trajectory of the electrode in a three-dimensional space in 1 mm intervals (Figure 1B).

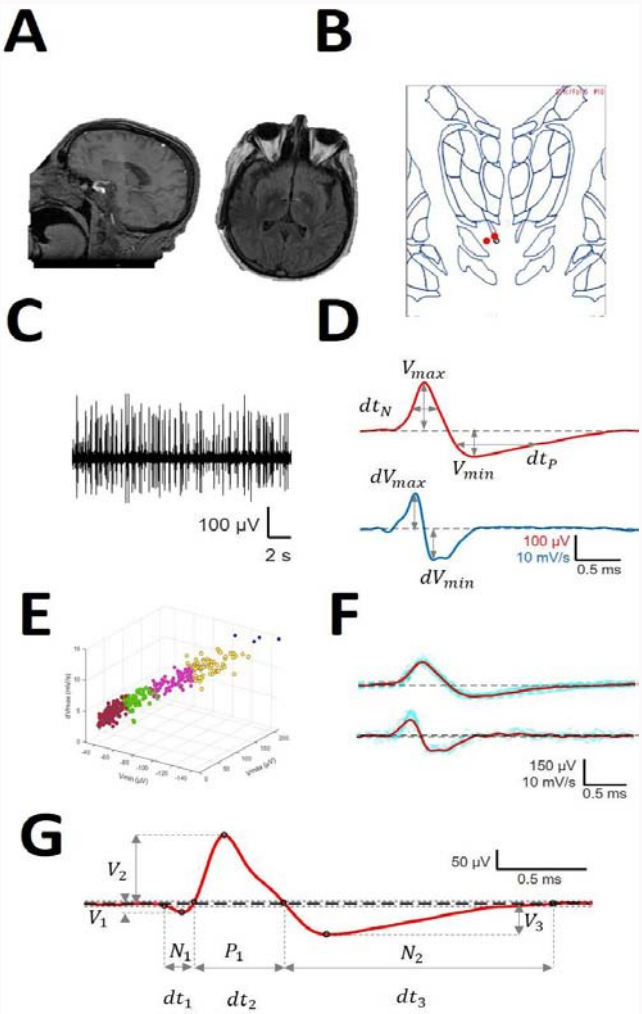

Figure 1: Clinical results and sorting for analysis of EAP. (A) Sagittal (left) and axial (right) MRi showing the placement of macroelectrode DBS (patient #2). (B) Frontal SW plate showing reconstruction of trajectory. Red dots indicated the location of lateral and medial microelectrodes. (C) Raw recording showing EAP as vertical lines of different amplitude. (D) EAP (upper row) and first derivative (lower row) showing the definitions of variables computed for sorting. (E) Clustering in different units (identified by different colors) of the raw trace. Only three dimensions are shown, although clusterization used up to 6. (F) mAP (upper row) and mDAP (lower row) in red obtained from AP and dAP of similar morphology (blue lines). (G) Example of mAP showing the definition of variables analyzed. Tick dashed line represents basal voltage, and thin dotted lines represent upper and lower thresholds used to characterize the structure. Dots are the fiducial points used to define amplitudes and phases.

Analysis of extracellular action potentials

Data were exported as ASCII files, and analyses were performed off-line. The recordings spanned 30 to 90 s (72 to 216 × 10^4 points). Raw recordings were digitally filtered at 500 Hz to 5 kHz using a 6^{th}-order Butterworth. We used zero-phase forward and reverse digital IIR filtering [20].

The polarity of the potentials was defined as Positive (P) upward and Negative (N) downward and was identified by order of appearance.

Algorithm for analysis:

Identification of EAPs. For every trace (Figure 1C), we computed a

Table 1: Demographic and clinical findings.

Patient	Age (yrs)	Sex	Intellectual capacity	Medical history	Medication	MRI
1	22	M	severe mental retardation	cluster headache, epilepsy	TPM, CLZ, RIS, LVM, OLZ	moderate diffuse cortico-subcortical atrophy; pineal cyst
2	22	M	moderate mental retardation	perinatal hypoxia	GBP, VPA, CYP, Li, OLZ	normal
3	48	M	moderate mental retardation	OCD, AVM, complex partial seizure	CBM, GBP, ZPX, CTP, CLZ	extensive encephalomalacia in right temporal lobe
4	37	F	severe mental retardation	epilepsy	LVM, OLZ, TPM, RIS, ARP	normal

ARP: Arpiprazole; AVM: Arterio-Venous Malformation; CBM: Carbamacepine; CLZ: Clorazepate; CTP: Citalopram; CYP: Cyproterone; GBP: Gabapentine; Li: Lithium; LVM: Levomepromazine; MRI: Magnetic Resonance Imaging; OCD: Obsessive-Compulsive Disorder; OLZ: Olanzapine; RIS: Risperidone; TPM: Topiramate; VPA: Valproic Acid; ZPX: Zuclopenthixol

maximum (V_+) and minimum (V_-) voltage threshold (in µV), defined as $V_\pm = \bar{V} \pm \sigma_V$, where $\bar{V}$ is the mean and σ_V is the standard deviation. EAPs must have two phases (depolarization and repolarization); therefore, we identified a tentative EAP when a positive/negative (P/N) phase was followed by a negative/positive (N/P) phase in a period of 0.3 ms to 0.6 ms. APs were defined as positive $\left(\frac{p}{|N|}>1\right)$ or negative $\left(\frac{p}{|N|}<1\right)$ according to the highest component identified.

Clustering was performed by an agglomerative hierarchical method, with distance between groups computed by farthest procedure. EAPs sharing similar morphologies were ascribed to the same neuron. For every EAP, we measured the maximum (V_{max}) and minimum voltages (V_{min}, in µV), durations of negative (dt_N) and positive phases at half-amplitude (dt_p in ms), and maximum (dV_{max}) and minimum values of the first derivative (dV_{min}, in mV/s). These measures can be considered as a 6-dimension vector for every k-AP, $AP_k = \left\{V^k_{max}, V^k_{min}, dt^k_N, dt^k_p, dV^k_{max}, dV^k_{min}\right\}$ (Figure 1D, 1E).

Construction of the mean Action Potential (mAP). All the EAPs from the same cluster were averaged to obtain a canonical waveform (Figure 1F, upper row), as were the derivatives to obtain the mean derivative (mDAP, 1F, lower row). A minimum of 10 EAPs was averaged. The first 300 µs (72 points) of baseline were used to compute the maximum (V_{AP+}) and minimum (V_{AP-}) voltage thresholds (in µV), defined as $V_{AP\pm} = \bar{V}_{AP} \pm 2.5\sigma_{AP}$, where $\bar{V}_{AP}$ is the mean and σ_{AP} the standard deviation. We used these thresholds to identify hallmark points in mAPs (Figure 1G). Every phase can be characterized by its polarity (P/N), duration (dt_i) and amplitude (V_i, i =1, 2, 3).

All analyses were performed in homemade MATLAB® R2018 scripts.

Statistics

Kurtosis (K) was computed for every group, and only values between 2 and 8 were acceptable for the homogeneous group [21]. Extreme outliers were removed. Statistical analysis was applied only to these groups.

Statistical comparisons between groups were performed using the Mann-Whitney U test or Kruskal-Wallis one-way ANOVA on ranks if normality failed. In the last case, Dunn's method was used for all pairwise post hoc comparisons. Normality was evaluated using the Kolmogorov-Smirnov test. The independence of variables (e.g., peak-to-peak action potential amplitude and amplitudes of depolarizing and repolarizing phases) was assessed by computing the rank (*rnk*) for the matrix containing observations (n) in rows and variables (p) in columns. Therefore, if *rnk*<p (considering that n>p always), then there would be some dependent variable that could be removed. However, when *rnk*=p, all the variables are independent and must be included in the analysis.

SigmaStat® 3.5 software (Point Richmond, USA) and MATLAB were used for statistical analyses. Pearson's correlation coefficient was used to study the linear dependence between variables. Linear regression significance was evaluated by means of a contrast hypothesis against the null hypothesis =0 using the formula

$$t = \frac{r\sqrt{n-2}}{\sqrt{1-r^2}} \qquad (3)$$

This describes a t-Student distribution with n-2 freedom degrees.

The significance level was set at p=0.05 and the results are shown as the mean ± SEM.

Ethics statement

The experimental procedure was approved by the medical ethics review board of the Hospital Universitario de La Princesa and was deemed "care as usual". Under these circumstances, written informed consent was not required.

Results

We have analysed MER from 2 mm above and 2 mm below the site of maximum physiological response to electrical stimulation [5], that was finally selected to DBS electrode implantation. In total, we have evaluated 159 mAP. Bearing in mind that every mAP is composed of 28.8 ± 11.6 APs, the total number of individual APs analysed was greater than 4550.

Types of extracellular action potentials

We analysed the structure of mAPs, defined as the arrangement of the parts composing the entire waveform. All the mAPs were positive. Only 16/159 (10.1%) mAPs showed 2 phases, being the majority cells with 3 phases structure. The most common type was P1P2N1, recorded in 104 cells (65.4%), and followed by N1P1N2, 39 cells (24.5%) and finally P1N1, only in 16 cells (10.1%). The most frequent had either a small positive or negative deflection before the main component (Figure 2). See Table S1 at Additional Materials for detailed numerical description of every type.

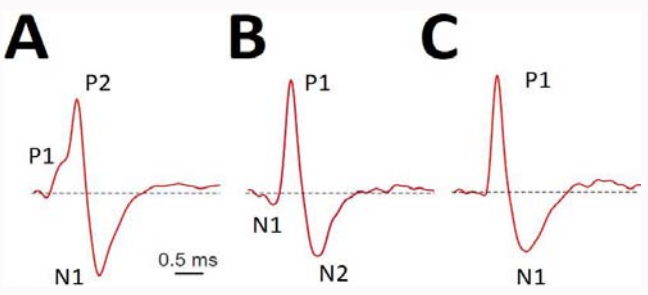

Figure 2: Amplitude-normalized canonical forms of mAP (A) P1P2N1, (B) N1P1N2 and (C) P1N1. The dashed line indicates the basal voltage. Positive (P) and negative (N) phases are indicated.

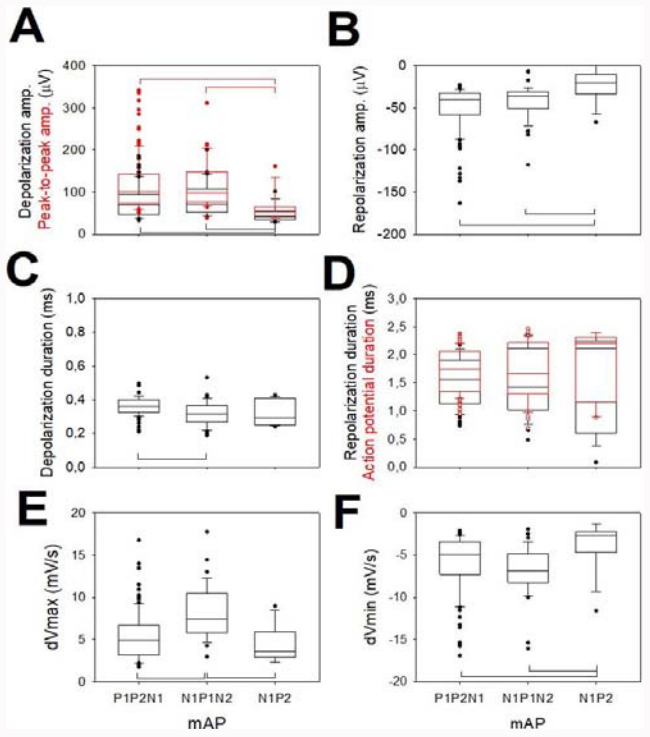

Figure 3: Box-plot graphs showing different properties of mAPs, indicated at x-axis. (A) Depolarization (black) and peak-to-peak (red) amplitudes; (B) amplitude repolarization; (C) depolarization duration; (D) repolarization (black) and action potential (red) duration; (E) dV_{max} and (F) dV_{min}. Horizontal brackets indicate the difference (Kruskal-Wallis One Way Analysis of Variance on Ranks, Dunn's test post-hoc) with post hoc test between pairs of variables. Red brackets refer to whole action potential variables (peak-to-peak and total duration).

The first phase for cells showed similar properties for absolute amplitude and duration, obviously with inverted polarity. Specifically, V1 was 15.8 ± 1.6 and -13.1 ± 1.4 µV respectively for P1P2N1 and N1P1N2 (p=0.839, Mann-Whitney U test) and dt_1 0.13 ± 0.01 and 0.14 ± 0.01 ms respectively (p=0.541, Mann-Whitney U test).

Canonical description of mAP

We have observed that most of the properties analysed were highly different according to ANOVA on ranks (p<0.001), although they were not different for all the pairwise post-hoc comparisons but were for most of them. It is observed from Figure 3 that there are not differences for amplitude for V2 and V3 and duration for phase V2 for P1P2N1/N1P1N2 mAPs, although the duration of V3 was longer for P1P2N1. In fact, the only difference for this kind of cells was the dV_{max}, higher for N1P1N2. On the contrary, most of the properties of amplitude and first derivative of P1N1 cells were different from P1P2N1 and N1P1N2 cells. However, the duration of both phases V2 and V3 were similar and, consequently the total duration of mAP.

From Figure 3 we can observe that amplitude of mAP (peak-to-peak measurement) depends mainly on V2 phase (depolarization), meanwhile, duration is directly dependent on dt_3 (repolarization phase).

Relationship between the first phase and rest of waves

We observed that most of the mAPs analyzed showed a first phase that was either positive or negative and smaller than the depolarizing phase. We correlated the maximum amplitudes of depolarization (V2) and repolarization (V3) (Figure 4A), and both of these phases

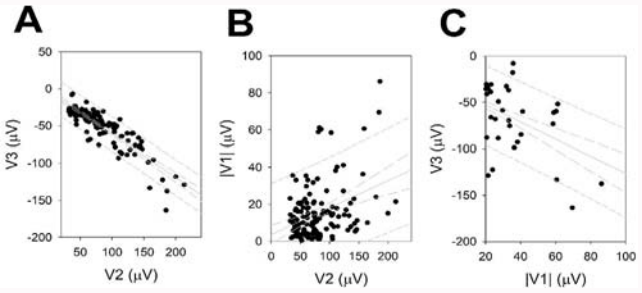

Figure 4: Linear regression for the maximum amplitude of the different phases of mAPs. (A) Depolarization (V2) *vs.* repolarization (V3); (B) depolarization (V2) *vs.* absolute value of phase 1 (|V1|) and (C) absolute value of phase 1 (|V1|) *vs.* repolarization (V3). Solid lines represent linear regressions; dashed lines represent 95% confidence band and dotted lines 95% prediction band.

with the absolute value of the first smaller one (V1|). The linear function adjusted for depolarizing and repolarizing phases was $V3(\mu V) = -0.585 \times V2 - 2.41$, r=0.888 (p<0.001, Student-t test). The linear regression between phase 1 and depolarization (Figure 4B) was $|V1|(\mu V) = 3.670 \times V2 + 0.14$, r=0.381 (p<0.01, Student-t test), and finally, the comparison between phase1 and repolarization (Figure 4C) gave $V3(\mu V) = -0.920 \times |V1| - 34.42$, r=0.533 (p<0.001, Student-t test). These results show that V1 is highly correlated with the other two phases forming the EAP and, therefore, probably pertain at the same process.

Although the correlation was higher for V2/V3, it was also highly significant for V1, which means that there is a correlation between the first phase and the repolarization/depolarization phases.

Discussion

To the best of our knowledge, this is the first work describing features of EAP from human PMH in detail. So far, only description of pattern discharge had been made at hypothalamus [3,5,8] but not detailed description of EAP were addressed. In animal recordings, the temporal structure of extracellular APs contains information about the intracellular spike [22]; therefore, we can hypothesize that the ionic conductances are different for each type of mAP.

Different methods for spike sorting have been described [23-27]. However, there is not a recognized-best-method. In this sense, clustering is a well-known, robust, and straightforward approach to grouping sets of data [10,28,29]. Sorting has been performed capturing features from the spikes shapes and later used for clustering the waveforms. The more discriminative features, the better the ability to distinguish the different spike shapes and we have used up to six independent variables to differentiate between EAP.

Recently our group has described the features of EAP from different identified thalamic nuclei [10]. We have noticed thalamic EAP with similar morphologies. In fact, we have observed in thalamus 78.7% of P1P2N1, 19.5% N1P1N2 and 6.3% P1N1. These percentages are very similar to found in this work (65.4%, 24.5% and 10.1% respectively for the same morphologies) and what is more relevant, the most prominent properties, as peak-to-peak amplitudes (146.7 ± 3.3/122.1 ± 3.9/78.8 ± 7.2 µV for P1P2N1/N1P1N2/P1N1) and total duration (2.83 ± 0.14/2.11 ± 0.03/1.99 ± 0.08 ms respectively) are similar to those described here (127.6 ± 8.7/124.7 ± 9.4/70.3 ± 8.6 µV for amplitude and 1.99 ± 0.28/1.97 ± 0.10/2.24 ± 0.18 ms for duration respectively for P1P2N1/N1P1N2/P1N1). Although a systematic statistical comparison was out of the scope of this work, because we

Table S1: Properties of types of EAP from PMH.

Properties	P1P2N1		N1P1N2		P1N1	
	$\bar{x} \pm SEM$	Med, [P25-P75]	$\bar{x} \pm SEM$	Med, [P25-P75]	$\bar{x} \pm SEM$	Med, [P25-P75]
N	104		39		16	
V1 (μV)	15.8 ± 3.8	11.3, [5.0-20.2]	-13.1 ± 1.4	-10.5, [-18.1- -6.1]	-	-
V2 (μV)	77.3 ± 2.8	70.1, [46.5-95.1]	81.9 ± 6.2	71.2, [52.8-104.8]	47.8 ± 4.9	41.2, [36.6-53.3]
V3 (μV)	-50.3 ± 6.3	-41.0, [-58.4- -32.3]	-42.8 ± 3.4	-36.4, [-50.1- -31.1]	-22.5 ± 5.4	-20.6, [-33.3- -11.0]
dt1 (ms)	0.13 ± 0.01	0.13, [0.09-0.16]	0.14 ± 0.01	0.13, [0.10-0.17]	-	-
dt2 (ms)	0.36 ± 0.04	0.36, [0.33-0.40]	0.32 ± 0.01	0.33, [0.27-0.36]	0.31 ± 0.02	0.29, [0.27-0.36]
dt3 (ms)	1.51 ± 0.04	1.56, [1.14-1.90]	1.51 ± 0.10	1.45, [1.04-2.10]	1.78 ± 0.19	2.57, [1.87-2.69]
Peak-peak (μV)	127.6 ± 0.87	109.0, [81.5-148.5]	124.7 ± 9.4	105.7, [83.6-154.6]	70.3 ± 8.6	62.3, [51.2-70.4]
dt_{AP} (ms)	1.99 ± 0.28	2.03, [1.56-2.41]	1.97 ± 0.10	1.96, [1.53-2.54]	2.24 ± 0.18	2.57, [1.87-2.69]
dV_{max} (mV/s)	5.4 ± 0.3	4.9, [3.2-6.7]	8.2 ± 0.5	7.4, [5.8-10.2]	4.3 ± 0.53	3.6, [3.0-5.1]
dV_{min} (mV/s)	-5.8 ± 0.3	-4.9, [-7.0- -3.5]	-6.7 ± 0.5	-6.9, [-8.1- -4.9]	-3.75 ± 0.72	-2.7, [-4.4- -2.4]

Med: Median; P25/P75: Percentile 25/75

need more cells from longer hypothalamic tracks to obtain a better picture of this complex nucleus. Nevertheless, it's quite interesting that EAP from such different structures, as several thalamic nuclei and PMH share similar properties in neurons. But, not all the properties obtained from thalamus were exactly super imposable to hypothalamus, e.g. no negative cells have been found from this structure, meanwhile we found 1.53% negative cells (P1N1P2 structure) at thalamus. However, considering the low frequency of negative cells at thalamus and the number of cells recorded at our work, we should expect around 2 to 3 negative cells, a number obviously too small that can be easily ignored.

It has been shown that the amplitude of extracellular spikes decreases monotonically with the distance from the soma [18,22]. This fact can explain the variation in amplitude because we can record neurons from a sphere of tissue approximately 5.23×10^5 μm^3 in volume. However, not only the distance to the microelectrode can be argued to modify the amplitude, but the net local field potential can also affect the amplitude of an EAP [22,30]. In fact, the total extracellular current injected to the volume recorded (e.g., by sources/sinks from surrounding tissue) can affect the amount of extracellular voltage generated by an extracellular current caused by an EAP. Nevertheless, despite these sources of variation, we have obtained highly significant differences in amplitude between types of mAP, probing that these differences are real and not induced by neuron-electrode distance.

We observed the presence of a small phase before depolarization in 89.9% of neurons. This first phase likely corresponds to the capacitive current. In fact, both numerical and experimental data have shown the presence of capacitive current prior to the large depolarizing phase [18,31,32]. We observed a highly significant correlation between the first phase amplitude and the two other phases of mAPs; therefore, we can reasonably argue that this small waveform is causally related to the action potential. It could be speculated that postsynaptic potentials may be responsible for this phase because, in fact these can be positive or negative. However, if this were the case, a greater variation would be expected, probably lacking of correlation with the other phases. However, the capacitive current is elicited by current spreading to dendrites from the soma and is always of the opposite polarity than the depolarization [18,31,32]. Surprisingly, we observed both opposite and similar polarities, which are difficult to collate with the capacitive current. The same finding was observed from thalamic cells. Settings from recording device (mainly filters) neither can explain the presence of this first phase. Therefore, we need more profound knowledge about EAP in humans before to identify a true cause of these potentials.

Conclusion

We have shown for first time that human hypothalmus near postero-medial nucleus have heterogeneous morphologies of EAP, probably conditioned by different ionic conductances. These EAP morphologies are partially, but not completely, shared with thalamic nuclei cells.

Acknowledgment

Authors want to acknowledge the collaboration during surgeries of neurosurgeons Marta Navas and Cristina Torres and anesthesiologists María Luisa Meilán and Eva de Dios.

Author Contributions

JP is responsible of the idea. LV-Z, EM-A and JP participated in data collection. JP developed the analytical methods and EM-A and LV-Z participated also in analysis and interpretation, and JP was responsible for manuscript preparation. All authors have approved the submitted version of this manuscript.

Funding

This work was financed by a grant from the Ministerio de Sanidad FIS PI17/02193, ISCIII (Instituto de Salud Carlos III) and partially supported by FEDER (Fonds Europeen de Developpement Economique et Regional).

References

1. Sano K, Mayanagi Y, Sekino H, Ogashiwa M, Ishijima B. Results of stimulation and destruction of the posterior hypothalamus in man. J Neurosurg. 1970;33:689-707.

2. Sano K, Mayanagi Y. Posteromedial hypothalamotomy in the treatment of violent, aggressive behaviour. Acta Neurochir Suppl (Wien). 1988;44:145-51.

3. Franzini A, Marras C, Ferroli P, Bugiani O, Broggi G. Stimulation of the posterior hypothalamus for medically intractable impulsive and violent behavior. Stereotact Funct Neurosurg. 2005;83:63-6.

4. Franzini A, Messina G, Cordella R, Marras C, Broggi G. Deep brain stimulation of the posteromedial hypothalamus: Indications, long-

term results, and neurophysiological considerations. Neurosurg Focus. 2010;29(2):E13.

5. Hernando V, Pastor J, Pedrosa M, Peña E, Sola RG. Low frequency bilateral hypothalamic stimulation for treatment of drug-resistant aggressiveness in a young man with mental retardation. Stereotact Funct Neurosurg. 2008;86(4):219-23.
6. Torres C, Sola RG, Pastor J, Pedrosa M, Navas M, García-Navarrete E, et al. Long-term results of posteromedial hypothalamic deep brain stimulation for patients with resistant aggressiveness. J Neurosurg. 2013;119(2):277-87.
7. Nieuwenhuys R, Voogd J, Van Huijzen C. The human central nervous system. 4th Ed. New York: Springer; 2008. p. 289-323.
8. Micieli R, Lopez Rios AL, Plata Aguilar R, Botero Posada LF, Hutchison WD. Single-unit analysis of the human posterior hypothalamus and red nucleus during deep brain stimulation for aggressivity. J Neurosurg. 2017;126(4):1158-64.
9. Heinricher MM. Microelectrode recording in movement disorder surgery. 1st Ed. New York: Thieme; 2004. p. 8-13.
10. Pastor J, Vega-Zelaya L. Features of action potentials from identified thalamic nuclei in anesthetized patients. Brain Sci. 2020;10(12):1002.
11. Vega-Zelaya L, Torres CV, Navas M, Pastor J. Neurophysiological characterization of thalamic nuclei in anaesthetized patients. Brain Sci. 2019;9(11):312.
12. Obwegeser AA, Uitti RJ, Turk MF, Strongosky AJ, Wharen RE. Thalamic stimulation for the treatment of midline tremors in essential tremor patients. Neurology. 2000;54(12):2342-4.
13. Wu D, Wang S, Stein JF, Aziz TZ, Green AL. Reciprocal interactions between the human thalamus and periaqueductal gray may be important for pain perception. Exp Brain Res. 2014;232(2):527-34.
14. Pastor J, Vega-Zelaya L. A new potential specifically marks the sensory thalamus in anaesthetized patients. Clin Neurophysiol. 2019;130(10):1926-36.
15. Shimamoto SA, Larson PS, Ostrem JL, Glass GA, Turner RS, Starr PA. Physiological identification of the human pedunculopontine nucleus. J Neurol Neurosurg Psychiatry. 2010;81(1):80-6.
16. Alam M, Sanghera MK, Schwabe K, Lütjens G, Jin X, Song J, et al. Globus pallidus internus neuronal activity: A comparative study of linear and non-linear features in patients with dystonia or Parkinson's disease. J Neural Transm. 2016;123(3):231-40.
17. Li X, Zhuang P, Hallett M, Zhang Y, Li J, Li Y. Subthalamic oscillatory activity in Parkinsonian patients with off-period dystonia. Acta Neurol Scand. 2016;134(5):327-38.
18. Gold C, Henze DA, Koch C, Buzsáki G. On the origin of the extracellular action potential waveform: A modeling study. J Neurophysiol. 2006;95(5):3113-28.
19. Hassler R. Introduction to stereotaxis with an atlas of the human brain. 1st Ed. New York: Thieme; 1959. p. 230–290.
20. Van Drongelen W. Signal processing for neuroscientists. 1st Ed. Amsterdam: Elsevier; 2007. p. 205-17.
21. Peña D, Prieto FJ. The kurtosis coefficient and the linear discriminant function. Stat Probab Lett. 2000;49(3):257-61.
22. Henze DA, Borhegyi Z, Csicsvari J, Mamiya A, Harris KD, Buzsáki G. Intracellular features predicted by extracellular recordings in the hippocampus *in vivo*. J Neurophysiol. 2000;84:390-400.
23. Laboy-Juárez KJ, Ahn S, Feldman DE. A normalized template matching method for improving spike detection in extracellular voltage recordings. Sci Rep. 2019;9:12087.
24. Chung JE, Magland JF, Barnett AH, Tolosa VM, Tooker AC, Lee KY, et al. A fully automated approach to spike sorting. Neuron. 2017;95:1381-94.
25. Rossant C, Kadir SN, Goodman DFM, Schulman J, Hunter MLD, Saleem AB, et al. Spike sorting for large, dense electrode arrays. Nat Neurosci. 2016;19:634-41.
26. Franke F, Quian Quiroga R, Hierlemann A, Obermayer K. Bayes optimal template matching for spike sorting – combining fisher discriminant analysis with optimal filtering. J Comput Neurosci. 2015;38(3):439-59.
27. Su CK, Chiang CH, Lee CM, Fan YP, Ho CM, Shyu LY. Computational solution of spike overlapping using data-based subtraction algorithms to resolve synchronous sympathetic nerve discharge. Front Comput Neurosci. 2013;7:149.
28. Ghahari A, Kumar SR, Badea TC. Identification of retinal ganglion cell firing patterns using clustering analysis supplied with failure diagnosis. Int J Neural Syst. 2018;28(8):1850008.
29. Mahallati S, Bezdek JC, Popovic MR, Valiante TA. Cluster tendency assessment in neuronal spike data. PLOS One. 2019;14(11):e0224547.
30. Anastassiou CA, Perin R, Buzsáki G, Markram H, Koch C. Cell type- and activity-dependent extracellular correlates of intracellular spiking. J Neurophysiol. 2015;114(1):608-23.
31. Holt GR, Koch C. Electrical interactions *via* the extracellular potential near cell bodies. J Comput Neurosci. 1999;6(2):169-84.
32. Bakkum DJ, Obien MEJ, Jäckel D, Radivojevic M, Jäckel D, Frey U, et al. The axon initial segment is the dominant contributor to the neuron's extracellular electrical potential landscape. Adv Biosyst. 2019;3(2);1800308.